Journal of Materials Chemistry A

PAPER

View Article Online
View Journal | View Issue

Cite this: J. Mater. Chem. A, 2016, 4, 12889

Unexpected highly reversible topotactic CO_2 sorption/desorption capacity for potassium dititanate†

Qianwen Zheng,[a] Liang Huang,[a] Yu Zhang,[a] Junya Wang,[a] Chen-Zi Zhao,[b] Qiang Zhang,[b] Weijie Zheng,[c] Dapeng Cao,[c] Dermot O'Hare[d] and Qiang Wang*[a]

Received 17th May 2016
Accepted 20th July 2016

DOI: 10.1039/c6ta04117e

www.rsc.org/MaterialsA

Potassium dititanate ($K_2Ti_2O_5$) was revealed to possess an unexpected, highly reversible CO_2 sorption/desorption capacity at *ca.* 750 °C, which is promising as a high-temperature CO_2 adsorbent for sorption enhanced hydrogen production (SEHP) processes. In contrast to numerous other adsorbents that are severely sintered during cycles at high temperatures, the CO_2 sorption/desorption cycles over $K_2Ti_2O_5$ exhibited a contrast particle size "break-down" process. The large $K_2Ti_2O_5$ particles gradually breakdown into $K_2Ti_2O_5$ nanofibers after 20 cycles, leading to a very stable CO_2 sorption/desorption performance with very rapid kinetics. A reversible CO_2 capture capacity as high as 7.2 wt% was achieved at 750 °C. Moreover, only 6 min is required for complete CO_2 desorption at 750 °C, indicating that this adsorbent can be practically run with a simple pressure swing sorption scheme. Surprisingly, an interesting structure switching phenomenon between $K_2Ti_2O_5$ and $K_2Ti_4O_9$ caused by CO_2 sorption and desorption was revealed. A detailed mechanism was proposed based on XRD, FTIR, SEM, HR-TEM, and SAED analyses and was further verified by density functional theory calculation. Considering its relatively high CO_2 capture capacity, superior cycling stability, and excellent regeneration ability, we believe $K_2Ti_2O_5$ offers significant potential as a practical, novel high-temperature CO_2 adsorbent.

1. Introduction

There is a general agreement that the CO_2 emission resulting from the burning of fossil fuels is one of the major reasons for the climate change.[1–3] It is expected that the energy demand will increase further by 53% by 2030, and fossil fuels will still be the dominant source in the next few decades.[4] In order to prevent these disastrous effects, there is now the need for a continuing and significant global effort to develop new technologies/processes for CO_2 capture, storage (sequestration) and utilization (CSU).[5–9] CSU is believed to be able to significantly reduce the amount of anthropogenic energy-related CO_2 emissions, and contribute to global climate change mitigation.[10] Among all the CO_2 capture technologies,[11] great attention has been devoted to pre-combustion CO_2 capture, particularly the sorption enhanced steam reforming (SESR) processes.[12–14]

Currently, more than 50 million tons of H_2 are produced annually, of which the majority is provided by a conventional steam methane reforming route because of the maturity of the technology and its favorable economics.[15] However, in order to further increase the H_2 production efficiency and lower the CO_2 emission, the SESR process has been developed recently, which is believed to be more economical, energy efficient, and environmentally friendly, as shown in reaction (1).[12,13] Since this reaction is equilibrium limited, it is impossible to achieve a complete conversion of CH_4 or CO in a single reactor under normal reaction conditions. However, if the CO_2 byproduct can be removed from the gas phase (*e.g.* by sorption on a solid CO_2 adsorbent), the normal equilibrium limits are removed and a complete conversion can be achieved. In addition, the process produces pure CO_2, which may be compressed and transported for further storage and utilization.[15,16] For the above mentioned SESR process, designing proper high-temperature CO_2 adsorbents is crucial for its practical implementation.

$$CH_4\,(g) + 2H_2O\,(g) + \text{adsorbent}\,(s) \leftrightarrow 4H_2\,(g) + \text{adsorbent–}CO_2\,(s) \quad (1)$$

To date, there are mainly three types of high-temperature CO_2 adsorbents that have been reported for SESR, which are

[a]College of Environmental Science and Engineering, Beijing Forestry University, 35 Tsinghua East Road, Haidian District, Beijing 100083, P. R. China. E-mail: qiang.wang.ox@gmail.com; qiangwang@bjfu.edu.cn; Tel: +86-13699130626

[b]Department of Chemical Engineering, Tsinghua University, 1 Tsinghua Road, Haidian District, Beijing 100084, P. R. China

[c]Division of Molecular and Materials Simulation, State Key Laboratory of Organic-Inorganic Composites, Beijing University of Chemical Technology, Beijing 100029, P. R. China

[d]Chemistry Research Laboratory, Department of Chemistry, University of Oxford, Mansfield Road, Oxford OX1 3TA, UK

† Electronic supplementary information (ESI) available. See DOI: 10.1039/c6ta04117e

CaO,[5,13] Li_2ZrO_3 (alkali zirconates),[17–19] and Li_4SiO_4 (alkali silicates).[20–22] Although great progress has been achieved with the above three types of adsorbents, each of them still has their own drawbacks, such as thermal sintering, low kinetics, *etc.* In this contribution, we are reporting the fourth example, $K_2Ti_2O_5$ (alkali dititanates) as a novel type of high-temperature CO_2 adsorbent. The present work reports the first study on the high-temperature CO_2 capture performance of potassium titanates ($K_2Ti_2O_5$, $K_2Ti_4O_9$, and $K_2Ti_6O_{13}$). Their CO_2 capture capacities were evaluated using thermogravimetric analysis (TGA) at 200–800 °C. The CO_2 sorption and desorption mechanism over the best adsorbent $K_2Ti_2O_5$ was investigated using XRD, FTIR, SEM, HR-TEM, SAED, and DFT calculations. The kinetics and cycling stability were also evaluated, and all results demonstrate that $K_2Ti_2O_5$ is a promising high-temperature CO_2 adsorbent for application in SEHP processes.

2. Experimental

2.1 Synthesis of potassium titanates

Three types of potassium titanates, $K_2Ti_2O_5$, $K_2Ti_4O_9$, and $K_2Ti_6O_{13}$ were synthesized by the solid state reaction method. Potassium carbonate (Sinopharm Chemical Reagent Co. Ltd.) and titanium dioxide (Sigma–Aldrich (Wuxi) Life Science & Technology Co. Ltd.) were mixed together, and ground into a fine powder in an agate mortar for a certain time. The molar ratios of $K_2CO_3 : TiO_2$ = 1 : 2, 1 : 4, 1 : 6 were chosen for $K_2Ti_2O_5$, $K_2Ti_4O_9$, and $K_2Ti_6O_{13}$, respectively. After that, they were calcined at 850, 970, and 1080 °C for 10.0 h in air to obtain $K_2Ti_2O_5$, $K_2Ti_4O_9$, and $K_2Ti_6O_{13}$, respectively, followed by cooling and crushing to fine powders.

2.2 Characterization of $K_2Ti_2O_5$

Powder X-ray diffraction (XRD) analyses were conducted in a Shimadzu XRD-7000 instrument in reflection mode with Cu Kα radiation and a power of 40 kV × 40 mA. Diffraction patterns were recorded within the range of 2θ = 5–80°, with a step size of 0.02°. The morphologies of synthesized potassium titanates were observed using scanning electron microscopy (SEM, Hitachi S-3400N II). Before observation, the dried samples were sputtered and coated with gold for ~120 s under an Ar atmosphere. High resolution transmission electron microscopy (HR-TEM) and selected area electron diffraction patterns (SAED) were performed on a JEM-2010F (JEOL, Japan) microscope with an accelerating voltage of 200 kV. Attenuated total reflectance-Fourier transform infrared spectroscopy (ATR-FTIR) spectra of the samples were measured using a Bruker Vertex 70 spectrophotometer. The thermal stability of the samples was determined using a Q50 TGA (TA Instruments) in N_2 with a flow rate of 40 mL min^{-1}. Typically, about 40 mg of sample were used for each run. The samples were placed in a Pt sample pan and heated from room temperature to 800 °C with a ramping rate of 10 °C min^{-1}.

2.3 CO_2 capture evaluation

Sorption of CO_2 on $K_2Ti_2O_5$, $K_2Ti_4O_9$, and $K_2Ti_6O_{13}$ was determined using a thermal gravimetric method on a Q50 TGA analyzer. All samples were pre-calcined at 750 °C for 1.0 h under a flow of 100% N_2 to remove the pre-absorbed species. CO_2 sorption experiments were carried out at certain temperatures for 2.0 h (*e.g.* 200, 300, 350, 700, 750, and 800 °C, respectively), and 1.0 atm with a constant flow of CO_2 (40 mL min^{-1}). Temperature programmed desorption (TPD) of CO_2 was carried out with a fixed bed reactor equipped with a tube furnace. The sample was heated up to 800 °C with a heating rate of 5 °C min^{-1}. The desorbed CO_2 was monitored using an on-line quadrupole mass spectrometer (Hiden, UK).

Cycling tests were also performed with a TGA analyzer. Approximately 40 mg of $K_2Ti_2O_5$ were loaded in a Pt pan. Before the cycling test, the sample was heated up to 750 °C at a ramping rate of 10 °C min under pure N_2. In a typical run, the sorption process was tested at 750 °C in CO_2 for 1.0 h. After sorption, the gas was switched to pure N_2 for desorption at 750 °C for 10 min. The CO_2 sorption and desorption cycles were repeated 20 times.

2.4 Calculation details

Theoretical calculations for $K_2Ti_2O_5$ and $K_2Ti_4O_9$ were based on density functional theory (DFT) implemented in the Vienna *Ab Initio* Simulation Package (VASP).[23,24] The projector augmented wave (PAW) method[25,26] was used in our calculation and the generalized gradient approximation (GGA) of the Perdew–Burke–Ernzerhof (PBE)[27] form was adopted to describe the exchange and correlation potentials. An energy cutoff of 500 eV was employed for the plane-wave basis throughout this work. All energy calculations were done with a Monkhorst–Pack *k*-point mesh of 7 × 7 × 5 with energy converged to 1.0×10^{-4} eV per atom.

3. Results and discussion

3.1 Synthesis and characterization of potassium titanates

Potassium titanates were synthesized using a simple solid state method, which is suitable for large scale preparation. In order to obtain well crystallized $K_2Ti_2O_5$, $K_2Ti_4O_9$, and $K_2Ti_6O_{13}$, the mixtures of TiO_2 and K_2CO_3 were calcined at 850, 970, and 1080 °C in air for 10.0 h, respectively. Fig. 1(a) shows the XRD patterns of the obtained potassium titanate samples; they all exhibit good consistency with the reported XRD patterns (PDF51-1890, PDF32-0861, and PDF40-0403, respectively). $K_2Ti_2O_5$ possesses unit cell dimensions a = 11.374 Å, b = 3.799 Å, c = 6.616 Å, β = 100.1°, the structure satisfies the space group of *C*2/*m*. On prolonged sintering of $K_2Ti_2O_5$, the (001) Bragg reflection is significantly stronger than the (111) reflection, due to texture (preferred orientation) effects. $K_2Ti_4O_9$ possesses unit cell dimensions a = 18.250 Å, b = 3.791 Å, c = 12.010 Å, and β = 106.4°, while $K_2Ti_6O_{13}$ possesses a monoclinic crystal structure with a = 15.593 Å, b = 3.796 Å, c = 9.108 Å, β = 99.78°, with a space group of *C*2/*m*. No impurity reflections were observed in these patterns, suggesting that the as-synthesized $K_2Ti_2O_5$, $K_2Ti_4O_9$, and $K_2Ti_6O_{13}$ are all phase pure. The inset of Fig. 1(a) shows the schematic structure of $K_2Ti_2O_5$. The titanium atoms are each co-ordinated to five oxygens grouped as a slightly distorted trigonal bipyramid, and this double unit forms an endless string elongated along the *y* direction. The layers are

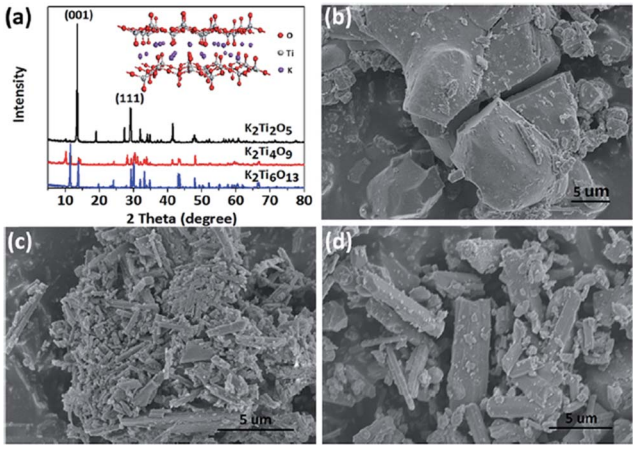

Fig. 1 (a) XRD patterns of synthesized $K_2Ti_2O_5$, $K_2Ti_4O_9$, and $K_2Ti_6O_{13}$, and the inset shows the schematic structure of $K_2Ti_2O_5$; (b) SEM image of synthesized $K_2Ti_2O_5$; (c) SEM image of synthesized $K_2Ti_4O_9$; (d) SEM image of synthesized $K_2Ti_6O_{13}$.

held together by the potassium atoms. According to theoretical calculation and model simulation for $K_2Ti_2O_5$, the bond distances of the five Ti–O bonds were obtained, which were 1.58, 1.91, 1.98, 1.99, and 1.98 Å, respectively.

The morphology of the synthesized potassium titanates were examined by SEM analysis (Fig. 1(b–d)). Fig. 1(b) indicates that irregular, flat, plate-like crystals of $K_2Ti_2O_5$ with particle size ranging from several micrometers to several-tens of micrometers were formed. $K_2Ti_4O_9$ formed whisker-type particles with an average width of 200 nm and a length of 5 μm, and $K_2Ti_6O_{13}$ exhibited rod-type particle morphology with an average width of 5 μm and a length of 10 μm. The SEM data show that the average particle size for both $K_2Ti_4O_9$ and $K_2Ti_6O_{13}$ are much smaller than $K_2Ti_2O_5$.

3.2 Decomposition and carbonation of potassium titanates

The decomposition and carbonation properties of the three potassium titanates were evaluated using TGA analysis in the presence of either N_2 or CO_2 (Fig. 2(a–c)). The TGA profiles of the decomposition processes suggest that all three potassium titanates possess very high thermal stability, with very little weight loss in the temperature range from 50 to 800 °C. For instance, the final weight losses for $K_2Ti_2O_5$, $K_2Ti_4O_9$, and $K_2Ti_6O_{13}$ were only 3.0, 0.4, and 0.1 wt%, respectively. This was to be expected since all these samples were synthesized at temperatures higher than 850 °C. For $K_2Ti_2O_5$, the major weight loss occurred in the temperature range of 50–200 °C, which is attributed to the desorption of surface water. During the carbonation processes, the trends in weight change for $K_2Ti_4O_9$ and $K_2Ti_6O_{13}$ were similar to those occurring during the decomposition processes. Both $K_2Ti_4O_9$ and $K_2Ti_6O_{13}$ resulted in weight loss, which was 0.5 and 0.2 wt%, respectively, while for $K_2Ti_2O_5$, it also displayed weight loss in the temperature range from 50–200 °C, and its weight then started to increase above 200 °C, due to the sorption of CO_2, and finally reached about 100.5%. These results demonstrate that the CO_2 sorption capacities of both $K_2Ti_4O_9$ and $K_2Ti_6O_{13}$ are very poor, and almost no CO_2 can be captured on either of these two potassium titanates. These data also suggest that only $K_2Ti_2O_5$ has the capability to capture CO_2, particularly in the temperature range of 600–800 °C. This is the first demonstration of CO_2 capture for $K_2Ti_2O_5$. Furthermore, among the different potassium titanates, the CO_2 capture capability is unique to $K_2Ti_2O_5$.

3.3 CO_2 capture performance of $K_2Ti_2O_5$

The carbonation experiments demonstrated that $K_2Ti_2O_5$ has great potential as a high-temperature CO_2 adsorbent. To illustrate the potential of $K_2Ti_2O_5$ for SEHP processes, its isothermal

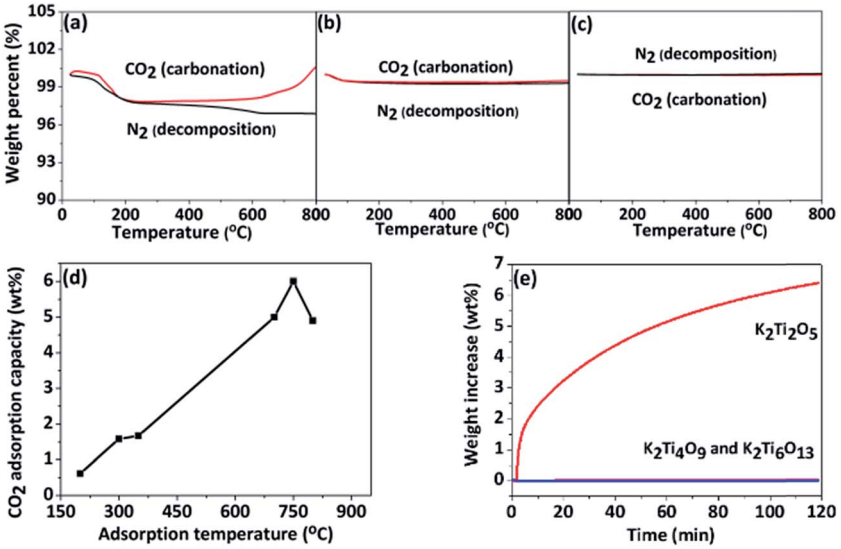

Fig. 2 TGA analyses of (a) $K_2Ti_2O_5$, (b) $K_2Ti_4O_9$, (c) $K_2Ti_6O_{13}$ during decomposition (in N_2) and carbonation (in CO_2) processes. (d) The effect of sorption temperature on the CO_2 capture capacity of $K_2Ti_2O_5$, (e) comparison of the CO_2 capture capacity of $K_2Ti_2O_5$, $K_2Ti_4O_9$, and $K_2Ti_6O_{13}$ at 750 °C.

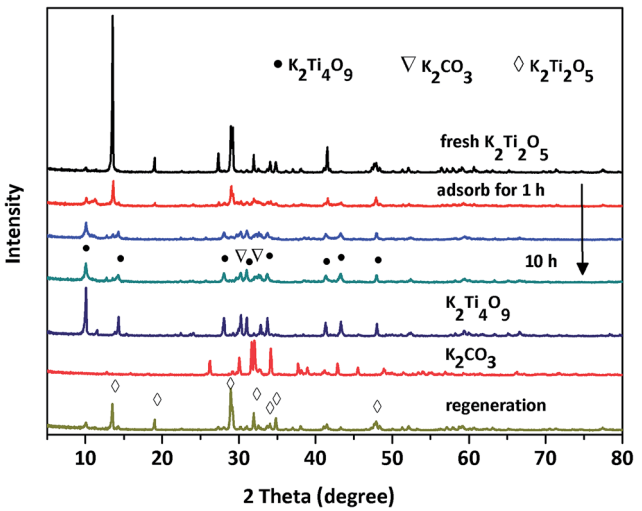

Fig. 3 XRD patterns of fresh $K_2Ti_2O_5$, CO_2-sorbed $K_2Ti_2O_5$ for 1.0, 5.0, and 10.0 h, fresh $K_2Ti_4O_9$, bulk K_2CO_3, and the regenerated $K_2Ti_2O_5$ sample.

CO_2 capture capacity was evaluated. Fig. 2(d) shows the effect of sorption temperature on the CO_2 capture capacity of $K_2Ti_2O_5$. The highest CO_2 uptake was achieved at around 750 °C. Before 750 °C, the sorption capacity increased with the increase in temperature, with values of 0.62, 1.58, and 1.67 wt% at 200, 300, and 350 °C, respectively. When the temperature was high, the CO_2 sorption capacity was notably improved, and reached 5.0 and 6.4 wt% at 700 and 750 °C, respectively. However, upon further increasing the sorption temperature to 800 °C, the CO_2 sorption capacity started to decrease (4.9 wt%). This is because the sorbed CO_2 started to desorb when the temperature was too high. These data indicate that the optimal CO_2 sorption temperature for $K_2Ti_2O_5$ is 750 °C. TGA data in Fig. S1† demonstrate that a rapid release of sorbed CO_2 can be achieved within 6.0 min after pure CO_2 was sorbed at 750 °C for 300.0 min. The excellent regeneration ability is also an important advantage for $K_2Ti_2O_5$. We have also compared the isothermal CO_2 capture capacity of $K_2Ti_2O_5$, $K_2Ti_4O_9$, and $K_2Ti_6O_{13}$ at 750 °C (Fig. 2(e)). It shows that only $K_2Ti_2O_5$ exhibits a rapid weight increase due to CO_2 sorption. The uptake exceeded 6.4 wt% after capturing CO_2 for 2.0 h. However, with the same temperature (750 °C) and time (2.0 h), neither $K_2Ti_4O_9$ nor $K_2Ti_6O_{13}$ exhibited any CO_2 capture. These data demonstrate that $K_2Ti_2O_5$ has an excellent CO_2 capture capacity and good potential for SEHP applications.

3.4 CO_2 sorption/desorption mechanism over $K_2Ti_2O_5$

In order to understand the CO_2 sorption and desorption mechanism, $K_2Ti_2O_5$ was exposed to CO_2 at 750 °C for a given time (1.0, 5.0, and 10.0 h), and the structural and morphological changes as a function of sorption time were monitored using XRD, FTIR, and SEM analyses. The XRD data in Fig. 3 clearly show that by the sorption of CO_2, the structure of $K_2Ti_2O_5$ gradually transformed into $K_2Ti_4O_9$ and K_2CO_3. With the increase in CO_2 sorption time, the characteristic Bragg reflections of $K_2Ti_2O_5$ disappear and concomitantly, the characteristic Bragg reflections of $K_2Ti_4O_9$ and K_2CO_3 grow in intensity. After CO_2 sorption for 10.0 h, the dominant Bragg reflections at $2\theta = 10.1°$ are much weaker and broader than that from a sample of $K_2Ti_4O_9$ synthesized by the traditional solid state route, indicating that the particle size of $K_2Ti_4O_9$ formed by CO_2 sorption is very small. After annealing the sample in pure N_2 at 750 °C, all the characteristic Bragg reflections of $K_2Ti_4O_9$ and K_2CO_3 disappeared and the structure transformed back into $K_2Ti_2O_5$, indicating that the structure transformation is reversible.

The process was also monitored by infrared spectroscopy, as shown in Fig. 4. After CO_2 sorption on $K_2Ti_2O_5$ at 750 °C for 1.0, 5.0, and 10.0 h, the characteristic peaks of $K_2Ti_4O_9$ were observed at 517, 771, and 939 cm^{-1}. The peaks at 517 cm^{-1} and 939 cm^{-1} were ascribed to the vibration of the Ti=O bond.[28] The peak at 771 cm^{-1} was due to the bridging μ^2-O–Ti vibration. Upon capturing CO_2, the vibration of CO_3^{2-} was observed at *ca.* 673 cm^{-1}.[29] Meanwhile, it is clear that the peaks centred at 1440 and 1050 cm^{-1} increased in intensity after capturing CO_2.[30] The 1430–1460 cm^{-1} peaks were probably caused by the presence of K_2CO_3.[31,32] After regenerating the CO_2-sorbed $K_2Ti_2O_5$ sample with pure N_2, most characteristic peaks of $K_2Ti_4O_9$ disappeared and a similar FTIR pattern to that of fresh $K_2Ti_2O_5$ was obtained, due to the existence of peaks at 673 and 771 cm^{-1}, the regeneration process might not be complete. These data further suggest that the CO_2 sorption and desorption over $K_2Ti_2O_5$ can be explained by a reversible structure switching mechanism between $K_2Ti_2O_5$ and $K_2Ti_4O_9$, accompanied by the formation of K_2CO_3.

The proposed reversible structural transformation during CO_2 sorption and desorption was also investigated using SEM (Fig. 5). Fresh $K_2Ti_2O_5$ showed flat, plate-like particles with relatively clean and smooth surfaces (Fig. 5(a)). However, after adsorbing CO_2 for 1.0 h, many cracks were found on the surface, indicating that the large particles had begun to disintegrate into

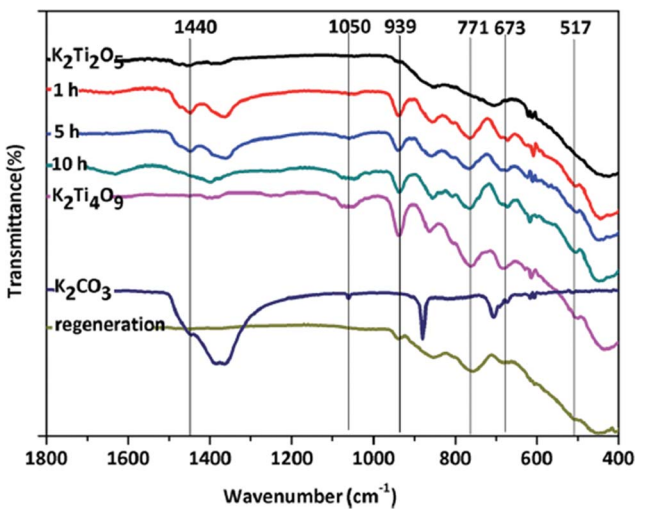

Fig. 4 FTIR patterns of fresh $K_2Ti_2O_5$, CO_2-sorbed $K_2Ti_2O_5$ for 1.0, 5.0, and 10.0 h, fresh $K_2Ti_4O_9$, bulk K_2CO_3, and the regenerated $K_2Ti_2O_5$ sample.

smaller pieces. With the increase in CO_2 sorption time, the particles became increasingly rough. After 10.0 h sorption, its structure was completely destroyed and collapsed into nanofibers corresponding to the formation of $K_2Ti_4O_9$ (Fig. 5(b–d)). The formation of nano-sized crystallites of $K_2Ti_4O_9$ is consistent with the XRD analysis. In order to prove that the morphology change is due to the sorption of CO_2, $K_2Ti_2O_5$ was tested under the same conditions (750 °C for 10.0 h) in N_2. Fig. S2† indicates that the morphology of $K_2Ti_2O_5$ treated in N_2, like fresh $K_2Ti_2O_5$, shows large particles with an average size of 5–10 μm.

HRTEM and SAED were employed to further verify the $K_2Ti_2O_5$–$K_2Ti_4O_9$ structure switching phenomenon during CO_2 sorption/desorption over $K_2Ti_2O_5$ (JCPDS, PDF51-1890) (Fig. 6). Fig. 6(a) and (b) show the TEM and SAED images of fresh $K_2Ti_2O_5$ before CO_2 sorption, in which the diffraction spots for the (020), (22$\bar{2}$) and (20$\bar{2}$) planes in $K_2Ti_2O_5$ were observed to be consistent with their interplanar spacing, with the [101] direction as the zone axis. The data confirmed the formation of the single crystals of $K_2Ti_2O_5$ before CO_2 sorption. Fig. 6(c) and (d) show the TEM and SAED images of freshly synthesized $K_2Ti_4O_9$. The diffraction spots for the (020), (211), (402), and (422) planes were clearly detected in the SAED pattern with the [10$\bar{2}$] direction as the zone axis. Fig. 6(e) and (f) show the TEM and SAED analyses of the $K_2Ti_2O_5$ sample after adsorbing CO_2 for 10.0 h. According to our previous XRD and FTIR analyses, the $K_2Ti_2O_5$ crystals transform into $K_2Ti_4O_9$ crystals due to the abstraction of K ions by CO_2. Thus, the CO_2 sorbed $K_2Ti_2O_5$ sample is expected to exhibit a diffraction pattern of $K_2Ti_4O_9$. The SAED diffraction pattern in Fig. 6(f) indeed confirmed our proposed mechanism, in which the diffraction spots of the (020) and [$\bar{4}$04] planes of $K_2Ti_4O_9$ were observed, with the [10$\bar{2}$] direction as the crystal zone axis.

In order to thoroughly demonstrate that the CO_2 sorption on $K_2Ti_2O_5$ is reversible, *i.e.*, that the formed $K_2Ti_4O_9$ and K_2CO_3 could transform back to $K_2Ti_2O_5$, a new experiment was designed. We deliberately mixed a proper ratio (1 : 1) of $K_2Ti_4O_9$ and K_2CO_3 and calcined the mixture at 750 °C for different times. The inverse process was analyzed using XRD (Fig. S3†), which clearly showed that the transformation between $K_2Ti_4O_9$ and $K_2Ti_2O_5$ occurs quickly, even within 1.0 h. For the mixture of $K_2Ti_4O_9$ and K_2CO_3, the characteristic reflections of both were clearly observed. With the increase in calcination time, the peaks for $K_2Ti_4O_9$ and K_2CO_3 (JCPDS, PDF16-0820) disappeared or significantly weakened, and concomitantly, the characteristic reflections of $K_2Ti_2O_5$ appeared and grew in intensity. Therefore, this experiment further verified the reversible structure switching mechanism between $K_2Ti_2O_5$ and $K_2Ti_4O_9$, accompanied by the formation of K_2CO_3.

According to the above discussions, a deeper understanding of the CO_2 sorption/desorption mechanism over $K_2Ti_2O_5$ was proposed, as shown in Fig. 7. $K_2Ti_2O_5$ exhibits a unique layered structure in which co-ordinate Ti atoms form a sheet of edge-sharing distorted bipyramids; the two-dimensional sheets or layers have the composition $(Ti_2O_5)^{2-}$. The layers are sandwiched by the potassium cations, which afford a curious unsymmetrical environment of eight oxygens, bearing only a superficial resemblance to the cubic site of the perovskite

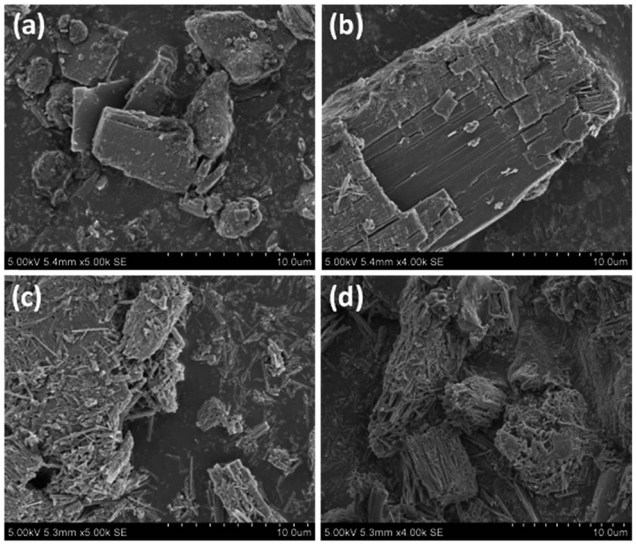

Fig. 5 SEM images of (a) fresh $K_2Ti_2O_5$, (b) CO_2-sorbed $K_2Ti_2O_5$ for 1.0 h, (c) CO_2-sorbed $K_2Ti_2O_5$ for 5.0 h, and (d) CO_2-sorbed $K_2Ti_2O_5$ for 10.0 h.

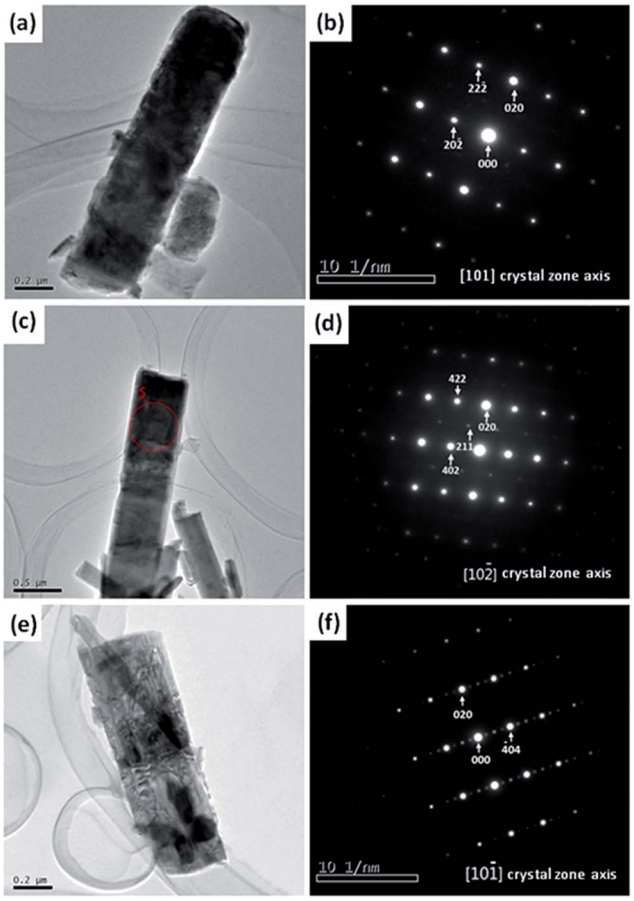

Fig. 6 HR-TEM images of (a) fresh $K_2Ti_2O_5$, (c) fresh $K_2Ti_4O_9$, and (e) CO_2-sorbed $K_2Ti_2O_5$ for 10.0 h, and SAED patterns of (b) fresh $K_2Ti_2O_5$, (d) fresh $K_2Ti_4O_9$, and (f) CO_2-sorbed $K_2Ti_2O_5$ for 10.0 h.

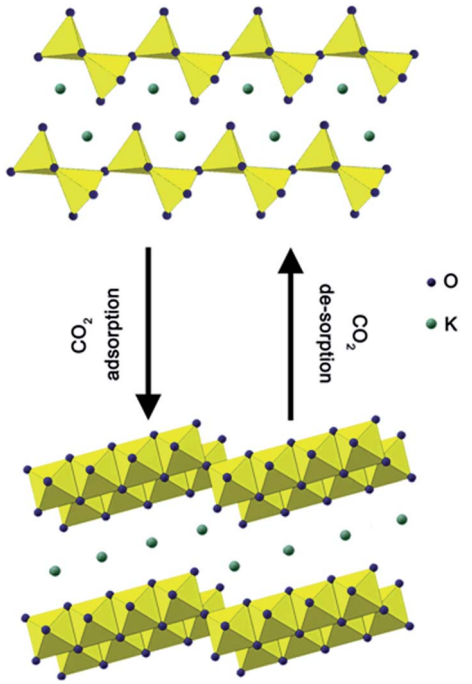

Fig. 7 The proposed mechanism of $K_2Ti_2O_5$–$K_2Ti_4O_9$ structure switching caused by CO_2 sorption and desorption.

structure.[33] Because the molecular size of CO_2 (~0.33 nm) is much smaller than the distance between adjacent $(Ti_2O_5)^{2-}$ sheets (0.65 nm), it is possible for CO_2 to penetrate into the inter-layers and react with K^+ located inside the layers at a certain temperature (600–800 °C). The shortage of potassium led $K_2Ti_2O_5$ to be transformed into $K_2Ti_4O_9$ with a low K/Ti value. The crystal structure of $K_2Ti_4O_9$ consists of many structural units connected through aligned TiO_6 octahedra. The four TiO_6 octahedra formed a framework by edge-sharing, and further constructed staggered sheets with a zigzag string by corner-sharing with the interlayer space of 0.88 nm.[34] Because K_2CO_3 possesses unit cell dimensions of $a = 5.640$ Å, $b = 9.831$ Å, and $c = 6.874$ Å (PDF87-0730), the formation of K_2CO_3 inside the layers finally led the large particles to disintegrate into nanofibers. By removing the sorbed CO_2, the released K reacts with $K_2Ti_4O_9$ once again to form $K_2Ti_2O_5$. This mechanism is also supported by our previous studies, in which we found a similar structure switching phenomenon between $K_2Ti_2O_5$ and $K_2Ti_6O_{13}$, induced by the gas phase sorption of molecular NO_x or SO_2 at 500–600 °C.[35,36] With CO_2, the reason $K_2Ti_2O_5$ changed into $K_2Ti_4O_9$, not $K_2Ti_6O_{13}$ is because the binding energy between K^+ and carbonate ions is lower than that with nitrate/sulfate ions. Revealing the structural changes during CO_2 adsorption and desorption is not only important for understanding and designing novel CO_2 adsorbents, but is also crucial for practical application. For instance, some key operating parameters, including theoretical CO_2 adsorption capacity, volume and heat changes during adsorption and desorption, and the highest temperature that can be applied, *etc.*, could be estimated from the structural change mechanism.

The energy changes during CO_2 sorption on $K_2Ti_2O_5$ were calculated using density functional theory (DFT), as shown in Fig. 8. The simulation results indicate that after losing two K atoms by adsorbing CO_2, if the resulting $K_2Ti_4O_9$* still maintains its previous structure, the system energy will be increased by 13.8 eV, which makes the system unstable. However, the transformation of $K_2Ti_4O_9$* into $K_2Ti_4O_9$ can lead to the system energy being reduced by 50.6 eV and achieving a steadier state. Thus, from the theoretical perspective, the DFT calculation further verified the feasibility of the proposed CO_2 sorption/desorption mechanism.

3.5 CO_2 sorption/desorption cycling test over $K_2Ti_2O_5$

For most of the high-temperature CO_2 adsorbents, such as CaO, alkali zirconates, and alkali silicates, the cycling stability is crucial for their practical application. Although their CO_2 capture capacity may be quite high, how to effectively prevent sintering is a major issue in long term use. In this contribution, the long-term stability of $K_2Ti_2O_5$ during CO_2 sorption–desorption cycles was also evaluated. In order to figure out the desorption conditions and explore the optimal desorption temperature of $K_2Ti_2O_5$, TPD of CO_2 was carried out. After adsorbing CO_2 at 750 °C, the sample was heated from room temperature to 800 °C with a heating rate of 5 °C min^{-1}. The desorbed CO_2 was monitored using an on-line quadrupole mass spectrometer. Fig. 9 shows that CO_2 desorption begins at 600 °C, with a peak temperature of 714 °C. The CO_2 sorption–desorption cycling test of $K_2Ti_2O_5$ was evaluated using a typical pressure swing sorption (PSA) process. The sorption was performed with pure CO_2 at 750 °C for 60.0 min and the desorption was performed with pure N_2 at 750 °C for 10.0 min. Fig. 9(b) shows the CO_2 sorption and desorption performance of $K_2Ti_2O_5$ during 20 cycles. There was no deterioration in the CO_2 uptake over 20 cycles. In contrast, the CO_2 uptake gradually increased within the first few cycles, and eventually became stable thereafter. As shown in Fig. 9(b), the CO_2 uptake increased from 3.9 wt% in cycle 1 to 7.2 wt% in cycle 6. After cycle 6, there was almost no change in CO_2 sorption capacity and it was maintained at *ca.* 7.2 wt%. Although the CO_2 capture capacity of $K_2Ti_2O_5$ is lower than that of CaO, $K_2Ti_2O_5$ exhibits superb

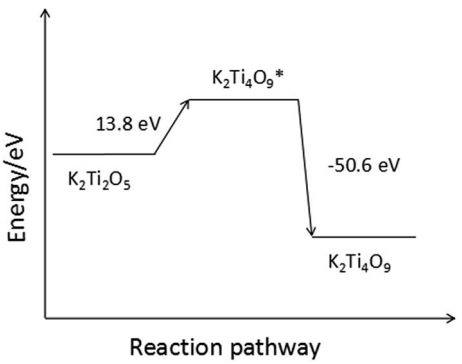

Fig. 8 The energy change of the CO_2 capture process calculated using the DFT method; $K_2Ti_4O_9$* means the intermediate state of $K_2Ti_2O_5$ after the sorption of CO_2.

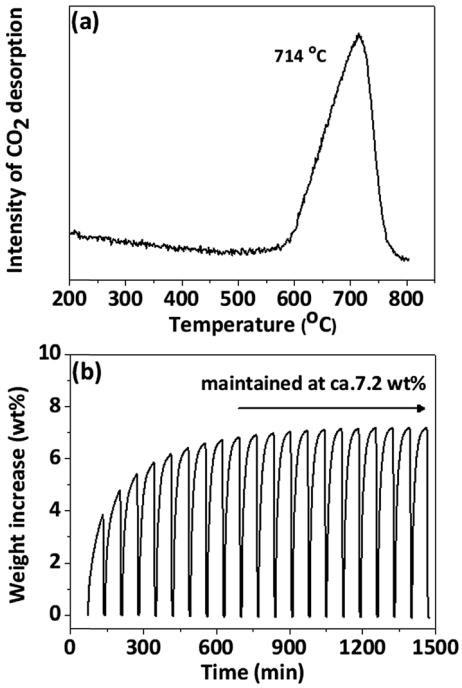

Fig. 9 (a) TPD analysis of the CO_2-sorbed $K_2Ti_2O_5$, and (b) the CO_2 sorption–desorption cycling test over $K_2Ti_2O_5$.

stability during CO_2 sorption–desorption cycles, which is critical for its practical application.

To clarify why the CO_2 capture capacity actually increased with the increase in cycle numbers, the $K_2Ti_2O_5$ samples after cycle 1, cycle 6, and cycle 20 were analyzed using SEM. The XRD data in Fig. 3 demonstrate that after the desorption of CO_2, the samples will transform back into $K_2Ti_2O_5$. Fig. 10 shows the morphological changes in $K_2Ti_2O_5$ after cycle 1, cycle 6, and cycle 20. Fresh $K_2Ti_2O_5$ shows big plate-like particles with clean and smooth surfaces (Fig. 10(a)), while on increasing the cycle number from 1 to 20, the particles gradually cracked down and formed $K_2Ti_2O_5$ nanofibers (Fig. 10(b–d)). Therefore, the improvement in CO_2 sorption capacity can be attributed to the morphological changes. Such formed $K_2Ti_2O_5$ nanofibers are more favorable for CO_2 sorption than the fresh $K_2Ti_2O_5$ whose particle size is much bigger.

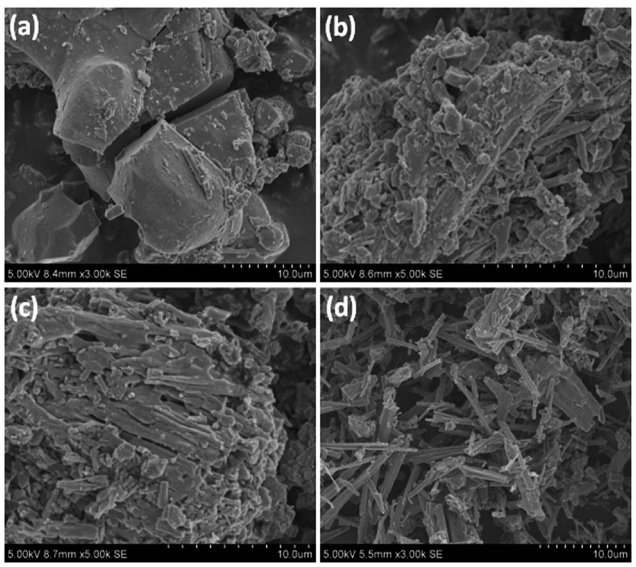

Fig. 10 SEM images of (a) fresh $K_2Ti_2O_5$, and $K_2Ti_2O_5$ after (b) cycle 1, (c) cycle 6, and (d) cycle 20.

4. Conclusion

In this contribution, in addition to the previously well studied Li_2ZrO_3 and Li_4SiO_4 as high-temperature CO_2 adsorbents, another type of alkali ceramic–potassium titanate, $K_2Ti_2O_5$, was investigated as a new type of high temperature CO_2 adsorbent, for the first time. TGA analyses in CO_2 (carbonation process) demonstrated that only $K_2Ti_2O_5$ has the capability to capture CO_2, particularly in the temperature range of 600–800 °C. Isothermal CO_2 sorption tests showed that the optimal sorption temperature for $K_2Ti_2O_5$ was 750 °C, with a capacity as high as 6.4 wt% after 2.0 h. By utilizing XRD, FTIR, SEM, TEM, and SAED analyses, the mechanism for the CO_2 sorption and desorption over $K_2Ti_2O_5$ was investigated, which can be explained by a reversible structure switching mechanism between $K_2Ti_2O_5$ and $K_2Ti_4O_9$, accompanied by the formation of K_2CO_3 species. The feasibility of the proposed CO_2 sorption/desorption mechanism was verified using DFT calculations. CO_2 sorption/desorption cycling tests proved that $K_2Ti_2O_5$ has excellent stability. In contrast to many adsorbents that deteriorate with cycles, the CO_2 uptake of $K_2Ti_2O_5$ gradually increased within the first few cycles, and eventually became stable afterwards (7.2 wt%). We also demonstrated that a rapid release of sorbed CO_2 can be achieved within only 6.0 min. The good CO_2 capture capacity, excellent cycling stability, and rapid regeneration indicate that $K_2Ti_2O_5$ could be a very promising high-temperature CO_2 adsorbent for the SEHP processes.

Acknowledgements

This work was supported by the Fundamental Research Funds for the Central Universities (2016ZCQ03), the National Natural Science Foundation of China (51572029, 51308045).

References

1 T. J. Crowley and R. A. Berner, *Science*, 2001, **292**, 870–872.
2 M. Meinshausen, N. Meinshausen, W. Hare, S. C. B. Raper, K. Frieler, R. Knutti, D. J. Frame and M. R. Allen, *Nature*, 2009, **458**, 1158–1163.
3 M. R. Raupach, G. Marland, P. Ciais, C. L. Quéré, J. G. Canadell, G. Klepper and C. B. Field, *Proc. Natl. Acad. Sci. U. S. A.*, 2007, **104**, 10288–10293.
4 D. M. D'Alessandro, B. Smit and J. R. Long, *Angew. Chem.*, 2010, **49**, 6058–6082.
5 Q. Wang, J. Luo, Z. Zhong and A. Borgna, *Energy Environ. Sci.*, 2011, **4**, 42–55.

6 M. E. Boot-Handford, J. C. Abanades, E. J. Anthony, M. J. Blunt, S. Brandani, N. Mac Dowell, J. R. Fernández, M.-C. Ferrari, R. Gross, J. P. Hallett, R. S. Haszeldine, P. Heptonstall, A. Lyngfelt, Z. Makuch, E. Mangano, R. T. J. Porter, M. Pourkashanian, G. T. Rochelle, N. Shah, J. G. Yao and P. S. Fennell, *Energy Environ. Sci.*, 2014, **7**, 130–189.
7 L. Huang, J. Wang, Y. Gao, Y. Qiao, Q. Zheng, Z. Guo, Y. Zhao, D. O'Hare and Q. Wang, *J. Mater. Chem. A*, 2014, **2**, 18454–18462.
8 R. S. Haszeldine, *Science*, 2009, **325**, 1647–1652.
9 S. Xiang, Y. He, Z. Zhang, H. Wu, W. Zhou, R. Krishna and B. Chen, *Nat. Commun.*, 2012, **3**, 954.
10 S. Chowdhury, G. K. Parshetti and R. Balasubramanian, *Chem. Eng. J.*, 2015, **263**, 374–384.
11 E. Andreoli, E. P. Dillon, L. Cullum, L. B. Alemany and A. R. Barron, *Sci. Rep.*, 2014, **4**, 7304.
12 D. P. Harrison, *Ind. Eng. Chem. Res.*, 2008, **47**, 6486–6501.
13 Z. Li, Y. Liu and N. Cai, *Int. J. Hydrogen Energy*, 2012, **37**, 11227–11236.
14 J. Wang, L. Huang, R. Yang, Z. Zhang, J. Wu, Y. Gao, Q. Wang, D. O'Hare and Z. Zhong, *Energy Environ. Sci.*, 2014, **7**, 3478–3518.
15 H. M. Jang, K. B. Lee, H. S. Caram and S. Sircar, *Chem. Eng. Sci.*, 2012, **73**, 431–438.
16 K. M. K. Yu, I. Curcic, J. Gabriel and S. C. Tsang, *ChemSusChem*, 2008, **1**, 893–899.
17 H. Pfeiffer, C. Vazquez, V. H. Lara and P. Bosch, *Chem. Mater.*, 2007, **19**, 922–926.
18 J. I. Ida and Y. S. Lin, *Environ. Sci. Technol.*, 2003, **37**, 1999–2004.
19 B. N. Nair, T. Yamaguchi, H. Kawamura and S. I. Nakao, *J. Am. Ceram. Soc.*, 2004, **87**, 68–74.
20 M. Kato, S. Yoshikawa and K. Nakagawa, *J. Mater. Sci. Lett.*, 2002, **21**, 485–487.
21 C. Gauer and W. Heschel, *J. Mater. Sci.*, 2006, **41**, 2405–2409.
22 K. Essaki, M. Kato and H. Uemoto, *J. Mater. Sci.*, 2005, **40**, 5017–5019.
23 G. Kresse and J. Hafner, *Phys. Rev. B: Condens. Matter Mater. Phys.*, 1994, **49**, 14251–14269.
24 G. Kresse and J. Furthmüller, *Phys. Rev. B: Condens. Matter Mater. Phys.*, 1996, **54**, 11169–11186.
25 P. E. Blöchl, *Phys. Rev. B: Condens. Matter Mater. Phys.*, 1994, **50**, 17953–17979.
26 G. Kresse and D. Joubert, *Phys. Rev. B: Condens. Matter Mater. Phys.*, 1999, **59**, 1758–1775.
27 B. Hammer, L. B. Hansen and J. K. Nørskov, *Phys. Rev. B: Condens. Matter Mater. Phys.*, 1999, **59**, 7413–7421.
28 W. Hou, Q. Yan, B. Peng and X. Fu, *J. Mater. Chem.*, 1995, **5**, 109–114.
29 X. Lv, Z. Chen, Y. Wang, F. Huang and Z. Lin, *ACS Appl. Mater. Interfaces*, 2013, **5**, 11271–11275.
30 J. Ortiz-Landeros, C. Gómez-Yáñez and H. Pfeiffer, *J. Solid State Chem.*, 2011, **184**, 2257–2262.
31 D. Yamaki, T. Nakazawa, T. Tanifuji, T. Aruga, S. Jitsukawa and K. Hojou, *J. Nucl. Mater.*, 2004, **329–333**, 1279–1282.
32 E. Carella and M. T. Hernandez, *Ceram. Int.*, 2014, **40**, 9499–9508.
33 S. Andersson and A. D. Wadsley, *Nature*, 1960, **187**, 499–500.
34 Y. Cao, K. Zhu, Q. Wu, Q. Gu and J. Qiu, *Mater. Res. Bull.*, 2014, **57**, 162–169.
35 Q. Wang, J. H. Sohn and J. S. Chung, *Appl. Catal., B*, 2009, **89**, 97–103.
36 Q. Wang and J. S. Chung, *Appl. Catal., A*, 2009, **358**, 59–64.

